

Chapter 4

Global Seismology of Sun-like Stars ¹

¹This chapter is from a paper accepted for publication in the *Astrophysical Journal* (Gizon & Solanki, 2003). Section 4.2 was published in *Astronomische Nachrichten* (Gizon, 2002).

4.1 Inclination of Stellar Rotation Axes

4.1.1 Introduction

For an Earth-based observer the rotation axis of the Sun is almost perpendicular to the line of sight. Traditionally, the solar rotation axis has been approximated to be exactly perpendicular to the ecliptic plane for helioseismic investigations of spatially-unresolved oscillation data. An exception concerns the search for oblique rotation of the Sun's core (Goode & Thompson, 1992; Gough et al., 1995). The rotation axes of stars are however randomly distributed in space. Since the visibility of the pulsation modes with various azimuthal orders m is a function of the angle between the rotation axis and the line of sight, i , this angle cannot be ignored in asteroseismology. The presence of random i values not only affects the method to measure oscillation mode parameters, but asteroseismology conversely provides us with the possibility of determining i , a parameter that in general is very poorly determined. Space missions such as COROT of CNES (Baglin et al., 2001) and Eddington of ESA (Favata et al., 2000) are expected to deliver the data necessary to do high-precision asteroseismology on a large number of stars.

The surface rotation rate of a star is one of its fundamental parameters and has been well studied. The standard method of deducing the rotation rate is to consider the widths of spectral lines. This technique only gives $v \sin i$, however, where v is the equatorial rotation velocity at the stellar surface. Asteroseismology can in principle provide measurements of the angular velocity, Ω , and of the inclination angle i . From these three measurements it is possible to determine the stellar radius, another fundamental parameter, without knowledge of stellar structure and evolution.

Knowledge of i is important not just for obtaining improved stellar parameters, but also in order to determine the masses of extra-solar planets. The standard technique used to detect such planets is to look for periodic Doppler shifts in the spectrum of the central star of the extra solar planetary system (Mayor & Queloz, 1995; Noyes et al., 1997; Marcy & Butler, 2000). This technique, however, only returns $M_p \sin i_p$, where M_p is the mass of the orbiting body and i_p is the inclination of the normal to its orbital plane relative to the line of sight. Clearly, the mass estimate obtained in this manner is a lower limit. Since i and i_p are expected to be similar

(see below) a knowledge of i would help to improve the mass estimates of extra solar planets considerably and would distinguish also misidentified brown dwarfs in orbits with small i_p from bona fide planets. In the solar system i and i_p differ by less than 10° for all the planets excluding Pluto. Also, currently favored theories of planetary system formation predict that the orbital plane of planets should nearly coincide with the equatorial plane of the central star (Safronov, 1972; Lissauer, 1993). An alternative technique for detecting planets involves looking for planetary transits in photometric data. So far this technique has uncovered only a couple of such systems (Charbonneau et al., 2000; Henry et al., 2000; Udalski et al., 2002; Konacki et al., 2003; Dreizler et al., 2003), compared to a total of over 100 planets detected using radial velocities. However, missions such as COROT, Eddington, and Kepler aim at discovering many such systems. Since for transiting planets i_p is known to high accuracy (Brown et al., 2001), a comparison with the independently measured i of the central stars would allow a direct test of the theoretical prediction that i_p and i are very similar. Clearly, there are many reasons to attempt to measure i .

Here we present a technique employing low-degree non-radial oscillations to determine i for sufficiently rapidly rotating stars. The technique makes use of the fact that the ratio of amplitudes of the $m = \pm 1$ and $m = 0$ components of dipole oscillations is a strong function of i . Similarly, the amplitudes of the peaks in quadrupole multiplets exhibit different dependences on i . This technique is thus similar to using the ratios of $\sigma(\Delta M_J = \pm 1)$ to $\pi(\Delta M_J = 0)$ components of Zeeman-split atomic transitions to determine the angle of the magnetic field vector relative to the line-of-sight, a standard procedure in Zeeman magnetometry. By studying solar dipole modes of oscillation, Gough et al. (1995) were able to measure the inclination of the Sun's rotation axis within 5° of the true value.

In this chapter we simulate a large number of realizations of oscillation power spectra seen in intensity with known values of the stellar rotation and of the inclination angle. We then fit a parametric model to each power spectrum with a maximum likelihood technique to estimate i , Ω , and other mode parameters. The distribution of the measured values of i indicates how precise a measurement can be. In order to assess the feasibility of the technique we adopt the pessimistic view

that only a single multiplet, $l = 1$ or $l = 2$, is observed. In practice, the information from tens of modes would be combined to better constrain i . Although we are investigating a problem which has not been studied before, we employ many results from helioseismology.

4.1.2 Effect of Rotation on Stellar Oscillations

Stars like the Sun undergo global acoustic oscillations driven by near-surface turbulent convection. The pulsation frequencies ω_{nl} of eigenmodes with radial order n and spherical harmonic degree l are characteristic of the spherically symmetric structure of a star (Brown & Gilliland, 1994). For distant Sun-like stars, observations are mostly sensitive to high-order acoustic modes with $l \leq 2$, i.e. radial, dipole, and quadrupole p modes. Because low-degree frequencies satisfy a relatively simple asymptotic relation (Tassoul, 1980) in which the large separation $\omega_{nl} - \omega_{n-1,l}$ and the small separation $\omega_{n0} - \omega_{n-1,2}$ depend weakly on n , the degree l of a multiplet can in principle be identified without ambiguity in the oscillation power spectrum (Fossat, 1981). A solar oscillation power spectrum for 200 days of observation of the total irradiance (Frohlich et al., 1997) is shown in Figure 4.1. Many attempts have been made to detect p modes on other Sun-like stars. So far they have only been clearly detected on α Cen A (Bouchy & Carrier, 2001; Schou & Buzasi, 2001; Bedding et al., 2002).

Rotation removes the $(2l + 1)$ -fold degeneracy of the frequency of oscillation of the mode (n, l) . The nonradial modes of a rotating star are thus labeled with a third index, the azimuthal order m , which takes integer values from $-l$ to $+l$. When the angular velocity of the star, Ω , is small, the effect of rotation on mode frequencies can be treated as a small perturbation. In the case of rigid-body rotation, and to a first order of approximation, the frequency of the mode (n, l, m) is given by (Ledoux, 1951):

$$\omega_{nlm} = \omega_{nl} + m\Omega(1 - C_{nl}). \quad (4.1)$$

The kinematic splitting, $m\Omega$, is corrected for the effect of the Coriolis force through the dimensionless quantity $C_{nl} > 0$ whose value depends on the oscillation eigenfunctions of the non-rotating star. High-order low-degree solar oscillations have $C_{nl} < 10^{-2}$; rotational splitting is dominated by advection. We note that the

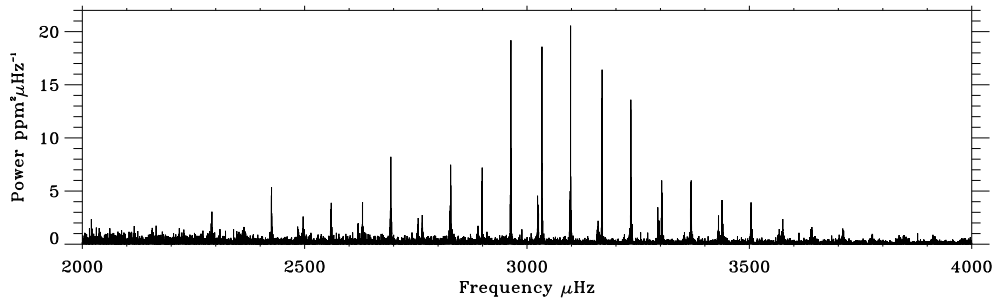


Figure 4.1: Solar oscillation power spectrum for 200 days of observation of the total irradiance (Frohlich et al., 1997). The data are from the VIRGO experiment aboard the ESA/NASA Solar and Heliospheric Observatory (SOHO). The global modes of oscillation are ordered in sequence: $(n - 1, l = 2)$, $(n, l = 0)$, and $(n, l = 1)$ with radial order n increasing with frequency. The large frequency separation is $(\omega_{n,l} - \omega_{n-1,l})/2\pi \sim 135 \mu\text{Hz}$ and the small separation is $(\omega_{n,l=0} - \omega_{n-1,l=2})/2\pi \sim 10 \mu\text{Hz}$.

rotation-induced frequency shift would not be linear in m if the angular velocity Ω were to vary with latitude (e.g. Hansen et al., 1977).

To the next order of approximation, centrifugal forces distort the equilibrium structure of the star. This results in an additional frequency perturbation (independent of the sign of m) which scales like the small parameter

$$\frac{\Omega^2 R^3}{\mathfrak{G}M}, \quad (4.2)$$

i.e. the ratio of the centrifugal to the gravitational forces at the stellar surface (Saio, 1981; Gough & Thompson, 1990). Here R denotes the radius of the star, M its mass, and \mathfrak{G} the universal constant of gravity. Second-order rotational effects are negligible in the Sun (Dziembowski & Goode, 1992). These effects are however significant for faster rotating Sun-like stars (Kjeldsen et al., 1998). Other perturbations, such as a large-scale magnetic field, may introduce further corrections to the pulsation frequencies (Gough & Thompson, 1990).

Here we only consider first-order rigid rotation, and substitute $\omega_{nl} + m\Omega$ for ω_{nlm} . Our purpose is to assess the feasibility of measuring the basic rotation parameters Ω and i . In an inertial frame \mathcal{R}' with polar axis coincident with the angular velocity vector $\mathbf{\Omega}$, scalar eigenfunctions are proportional to a spherical harmonic function $Y_l^m(\theta', \phi')$, where θ' and ϕ' are the co-latitude and longitude defined in

the spherical-polar coordinate system associated with \mathcal{R}' . Under the approximation that the intensity fluctuation due to a mode of oscillation is proportional to a scalar eigenfunction measured at the stellar surface (such as the Lagrangian pressure perturbation), the brightness variations due to the free oscillations of a star may be written as a linear combination of eigenmodes:

$$I'(t, \theta', \phi') = \Re \sum_{nl} \sum_{m=-l}^l A_{nlm} Y_l^m(\theta', \phi') e^{i\omega_{nlm}t}, \quad (4.3)$$

where A_{nlm} are complex amplitudes, t denotes time, and \Re takes the real part of the expression. A more accurate expression for I' requires an explicit relationship between mode displacement and light-flux perturbation (e.g. Toutain & Gouttebroze, 1993).

To obtain the intensity that an Earth-based observer would measure, it is convenient to transform to an inertial frame \mathcal{R} with polar axis pointing toward the observer, inclined by the angle i with respect to Ω . Co-latitude θ and longitude ϕ are spherical-polar coordinates defined in \mathcal{R} . For an appropriate choice of longitude origins, spherical harmonics expressed in \mathcal{R}' and \mathcal{R} are related linearly according to (Messiah, 1959):

$$Y_l^m(\theta', \phi') = \sum_{m'=-l}^l Y_l^{m'}(\theta, \phi) r_{m'm}^{(l)}(i), \quad (4.4)$$

where the rotation matrix $\mathbf{r}^{(l)}$ is real and unitary. According to Wigner's formula (see Messiah, 1959) each rotation matrix element can be written explicitly as a homogeneous polynomial of total degree $2l$ in the two variables $\sin(i/2)$ and $\cos(i/2)$. Inserting equation (4.4) into equation (4.3) we obtain intensity variations expressed in the frame with polar axis ($\theta = 0$) pointing toward the observer:

$$I(t, \theta, \phi) = \Re \sum_{nlmm'} A_{nlm} Y_l^{m'}(\theta, \phi) r_{m'm}^{(l)}(i) e^{i\omega_{nlm}t}. \quad (4.5)$$

The spherical harmonic projection (l, m') is given by a linear combination of eigenmodes (l, m) . From the above equation, we derive the observed disk-integrated

intensity signal, $I(t)$:

$$I(t) = \int_0^{2\pi} d\phi \int_0^{\pi/2} d\theta I(t; \theta, \phi) W(\theta) \cos \theta \sin \theta, \quad (4.6)$$

where $W(\theta)$ is the limb-darkening function. Because the function $Y_l^{m'}(\theta, \phi)$ is proportional to $\exp(im'\phi)$, components with $m' \neq 0$ vanish upon integration over azimuth, and

$$I(t) = \Re \sum_{nlm} V_l A_{nlm} r_{0m}^{(l)}(i) e^{i\omega_{nlm}t}, \quad (4.7)$$

with the visibility factor V_l given by

$$V_l = 2\pi \int_0^{\pi/2} Y_l^0(\theta) W(\theta) \cos \theta \sin \theta d\theta. \quad (4.8)$$

For each (l, n) there are $2l + 1$ visible peaks in the power spectrum; as is expected for a steady perturbation such as rotation. The quantity V_l^2 is an estimate of the geometrical visibility of the total power in a multiplet (l, n) as a function of l . The solar limb darkening function quoted by Pierce (2000) implies $(V_1/V_0)^2 = 0.50$ and $(V_2/V_0)^2 = 0.17$. These estimates are crude (see Toutain & Gouttebroze, 1993). However, the ratios V_l/V_0 are unimportant to the present study as we are interested in the relative power between azimuthal modes with common values of l and n .

Assuming that there is energy equipartition between modes with different azimuthal order, we write amplitudes A_{nlm} in the form

$$A_{nlm} = |A_{nl}| e^{i\phi_{nlm}}, \quad (4.9)$$

where the magnitude $|A_{nl}|$ is independent of m , and ϕ_{nlm} is an arbitrary phase. Using this assumption, consistent with the solar data, together with equation (4.7), we find that the dependence of mode power on azimuthal order m is given by

$$\mathcal{E}_{lm}(i) = [r_{0m}^{(l)}(i)]^2. \quad (4.10)$$

Matrix elements $r_{0m}^{(l)}(i)$ are explicitly given by Messiah (1959) in terms of associated

Legendre functions, P_l^m :

$$\mathcal{E}_{lm}(i) = \frac{(l - |m|)!}{(l + |m|)!} \left[P_l^{|m|}(\cos i) \right]^2. \quad (4.11)$$

The above equation links mode visibility to inclination angle i (see also Dziembowski, 1977; Toutain & Gouttebroze, 1993). It provides the basic information required to later extract i from photometric measurements. It is however unknown whether the key assumption, equation (4.9), remains valid for very fast rotators as rotation affects convection and therefore the mechanism by which acoustic modes are excited. For dipole multiplets, $l = 1$, the observed mode power (Eq. [4.11]) is given by

$$\mathcal{E}_{1,0}(i) = \cos^2 i \quad (4.12)$$

$$\mathcal{E}_{1,\pm 1}(i) = \frac{1}{2} \sin^2 i. \quad (4.13)$$

For quadrupole multiplets, $l = 2$, we have

$$\mathcal{E}_{2,0}(i) = \frac{1}{4} (3 \cos^2 i - 1)^2, \quad (4.14)$$

$$\mathcal{E}_{2,\pm 1}(i) = \frac{3}{8} \sin^2(2i), \quad (4.15)$$

$$\mathcal{E}_{2,\pm 2}(i) = \frac{3}{8} \sin^4 i. \quad (4.16)$$

It is worth noting the symmetries $\mathcal{E}_{lm}(-i) = \mathcal{E}_{lm}(\pi - i) = \mathcal{E}_{lm}(i)$. Knowledge of $\mathcal{E}_{lm}(i)$ is not enough to fully specify the direction and sense of the rotation axis, but only $|i|$ modulo π . When the rotation axis is aligned with the line of sight ($i = 0 \bmod \pi$), only the mode $m = 0$ is visible and rotation cannot be inferred. Notice also that $\sum_m \mathcal{E}_{lm}(i) = 1$, so that \mathcal{E}_{lm} represents the relative power in the mode m within a multiplet (n, l) .

4.1.3 Modeling Oscillation Power Spectra

In the previous section we studied the intensity variations due to the free oscillations of a star with an arbitrary orientation of the rotation axis. We found that the

brightness variations can be approximated by

$$I(t) = \sum_{m=-l}^l \sqrt{\mathcal{E}_{lm}(i)} \cos[(\omega_{nl} + m\Omega)t + \phi_m], \quad (4.17)$$

when considering only the contribution from a single multiplet (n, l) . The observed power in the azimuthal component m is given by $\mathcal{E}_{lm}(i)$, and ϕ_m is an arbitrary phase. In Sun-like stars, oscillations are however excited by near-surface turbulent convection. The above model is too simple as it ignores the stochastic nature of stellar pulsations (Woodard, 1984). Oscillations also have a finite lifetime determined by their interaction with convection. In this section we give a more realistic description of the statistical properties of the oscillation signal in Fourier space.

The observed brightness variations of a star are presumed to be given by the function $I(t)$ recorded over a large observation time interval of length T , at a sufficiently high cadence (say less than 1 min). Since pulsations are forced by turbulence, the signal is a random sample drawn from some probability distribution. Neglecting edge effects introduced by the time window, we assume that $I(t)$ is a stationary process. We denote by $I(\omega_j)$ the FFT of $I(t)$ sampled at the angular frequency $\omega_j = 2\pi j/T$. A random variable is fully specified by its expectation value, E , and higher-order moments (in the sense of ensemble averages). Here, $I(\omega_j)$ is complex with zero mean, $E[I(\omega_j)] = 0$, and stationarity implies that frequency bins are uncorrelated:

$$E[I^*(\omega_j) I(\omega_{j'})] = 0 \quad \text{for } j \neq j'. \quad (4.18)$$

Foglizzo et al. (1998) showed that low-degree modes are essentially uncorrelated. This is a consequence of the fact that there is a very large number of excitation events per damping time. The central limit theorem ensures that mode amplitudes converge to independent Gaussian distributions. The signal $I(\omega_i)$ can thus be modeled by a sum of independent complex Gaussian random variables:

$$I(\omega_j) = \sum_m \sigma_m(\omega_j) \mathcal{N}_{m,j} + \sigma^n \mathcal{N}_j^n. \quad (4.19)$$

The symbol \mathcal{N} denotes a complex Gaussian random variable with zero mean and unit variance, $E[\mathcal{N}^* \mathcal{N}] = 1$. The standard deviation of a mode amplitude, denoted

by the function $\sigma_m(\omega)$, is large for ω near the resonant frequency $\omega_{nl} + m\Omega$ (see below). The distributions $\mathcal{N}_{m,j}$ are all independent of each other. The additional term $\sigma^n \mathcal{N}_j^n$ denotes uncorrelated Gaussian noise with standard deviation σ^n . The origin of this noise is both stellar (convection) and instrumental (e.g. photon noise). For simplicity, the noise level, σ^n , is assumed to be frequency independent over a small frequency interval around ω_{nl} .

In order to obtain $\sigma_m(\omega)$ one should in principle solve the inhomogeneous wave equations once a model for wave damping and excitation has been specified. Here, however, we parametrize the variance σ_m^2 in the form

$$\sigma_m^2(\omega) = S \mathcal{E}_{lm}(i) L_{nl}(\omega - m\Omega). \quad (4.20)$$

The constant S gives the overall amplitude of the power, and the weights $\mathcal{E}_{lm}(i)$ give the m -dependent visibility as a function of inclination angle i (cf. § 4.1.2). The line shape, $L_{nl}(\omega)$, is a real positive function which becomes large for ω near the resonant frequency ω_{nl} . We choose the standard Lorentzian line profile (e.g. Anderson et al., 1990) appropriate for describing an exponentially damped oscillator:

$$L_{nl}(\omega) = \left[1 + \left(\frac{\omega - \omega_{nl}}{\Gamma/2} \right)^2 \right]^{-1}, \quad (4.21)$$

where the damping rate Γ represents the full width at half maximum of $L_{nl}(\omega)$. Notice that equation (4.21) only gives the positive-frequency part of the spectrum; the negative-frequency part does not contain extra information and can be deduced from the relation $I(-\omega) = I^*(\omega)$.

Since the sum of independent Gaussian random variables is a Gaussian variable, the Fourier spectrum (Eq. [4.19]) at frequency ω_j can be written in terms of a single complex normal distribution, \mathcal{N}_j :

$$I(\omega_j) = \left[S \sum_m \mathcal{E}_{lm}(i) L_{nl}(\omega_j - m\Omega) + N \right]^{1/2} \mathcal{N}_j. \quad (4.22)$$

We introduced the notation $N = (\sigma^n)^2$. The traditional method to generate a complex Gaussian distribution is called the Box-Muller method. Given a uniform

distribution on $[0, 1]$, U_j , and a uniform distribution on $[0, 2\pi]$, Θ_j , the random variable

$$\mathcal{N}_j = \sqrt{-\ln U_j} e^{i\Theta_j} \quad (4.23)$$

is complex Gaussian with independent real and imaginary parts and unit variance. From equations (4.22) and (4.23), we see that a realization of the power spectrum is given by

$$P(\omega_j) = |I(\omega_j)|^2 = -\ln(U_j) \mathcal{P}(\omega_j), \quad (4.24)$$

where \mathcal{P} is the expectation value of the power spectrum,

$$\mathcal{P}(\omega_j) = S \sum_m \mathcal{E}_{lm}(i) L_{nl}(\omega_j - m\Omega) + N. \quad (4.25)$$

We now have an expression for generating realizations of a stellar oscillation power spectrum. Because $L_{nl}(\omega_{nl}) = 1$, it makes sense to refer to S/N as the signal-to-noise ratio in the power spectrum. Since $-\ln(U_j)$ is an exponential distribution with unit mean and variance, the probability density function of the random variable $P(\omega_j)$ is given by

$$f(P_j) = \frac{1}{\mathcal{P}(\omega_j)} \exp\left(-\frac{P_j}{\mathcal{P}(\omega_j)}\right), \quad (4.26)$$

where $f(P_j)$ describes the probability that $P(\omega_j)$ takes a particular value P_j (Woodard, 1984; Duvall & Harvey, 1986).

Figure 4.2 shows plots of the expectation value of the power spectrum, $\mathcal{P}(\omega)$, for various values of the inclination angle i . The left panels in Figure 4.2 are for dipole multiplets $l = 1$, and the right panels for quadrupole multiplets $l = 2$. In these plots the parameters are $\Gamma = \Gamma_\odot$ and $\Omega = 6\Omega_\odot$, where $\Gamma_\odot/2\pi = 1 \mu\text{Hz}$ and $\Omega_\odot/2\pi = 0.5 \mu\text{Hz}$ are characteristic solar values for the line width and the angular velocity. For noiseless data, the dependence of the power at different frequencies on i is clearly evident, and it is possible to distinguish between different i values relatively easily.

To illustrate the effect of stochastic excitation, Figure 4.3 shows two realizations, $P(\omega)$, of an $l = 2$ power spectrum for $i = 30^\circ$ and $i = 80^\circ$, together with the expectation values denoted by the thick curves. A solar-like background noise was

prescribed ($S/N = 100$). Although realization noise is important, the two spectra can be distinguished from each other.

In the previous section, we described a simple statistical model for the stellar oscillation power spectrum. This model depends on a minimal set of physical parameters (ω_{nl} , Γ , Ω , i) and the overall signal and noise levels (S, N). In this section, we describe an algorithm which allows to estimate these parameters from a realization of the power spectrum. We use the maximum likelihood method which is commonly used in helioseismology (e.g. Anderson et al., 1990; Schou, 1992; Toutain & Appourchaux, 1994; Appourchaux et al., 1998, 2000).

We consider a section of the spectrum that includes the $2l + 1$ peaks of a given multiplet (l, n). The spherical harmonic degree l is either 1 or 2. We denote by $\boldsymbol{\lambda}$ the set of parameters that we want to estimate:

$$\boldsymbol{\lambda} = \{i, \Omega, \omega_{nl}, \Gamma, S, N\}. \quad (4.27)$$

Maximum likelihood estimators involve specifying the joint probability density function for the sample data $\{P_j\}$. For a given frequency ω_j , the probability that the power takes the particular value P_j is given by the probability density function, $f(P_j)$ (see Eq. 4.26). We write $f(P_j|\boldsymbol{\lambda})$ to indicate the dependence on the parameters $\boldsymbol{\lambda}$. Because frequency bins are independent, the joint probability density function is simply the product of $f(P_j|\boldsymbol{\lambda})$ for the index j spanning the frequency interval of interest. The likelihood function $F(\boldsymbol{\lambda})$ is another name for the joint probability function evaluated at the sample data

$$F(\boldsymbol{\lambda}) = \prod_j f(P_j|\boldsymbol{\lambda}). \quad (4.28)$$

The basic idea of maximum likelihood estimation is to choose estimates $\boldsymbol{\lambda}^*$ so as to maximize the likelihood function. In practice, one minimizes

$$\mathcal{L}(\boldsymbol{\lambda}) = -\ln F(\boldsymbol{\lambda}). \quad (4.29)$$

This gives the same result since the logarithm is a monotonic increasing function. The probability of observing the sample values is greatest if the unknown parameters

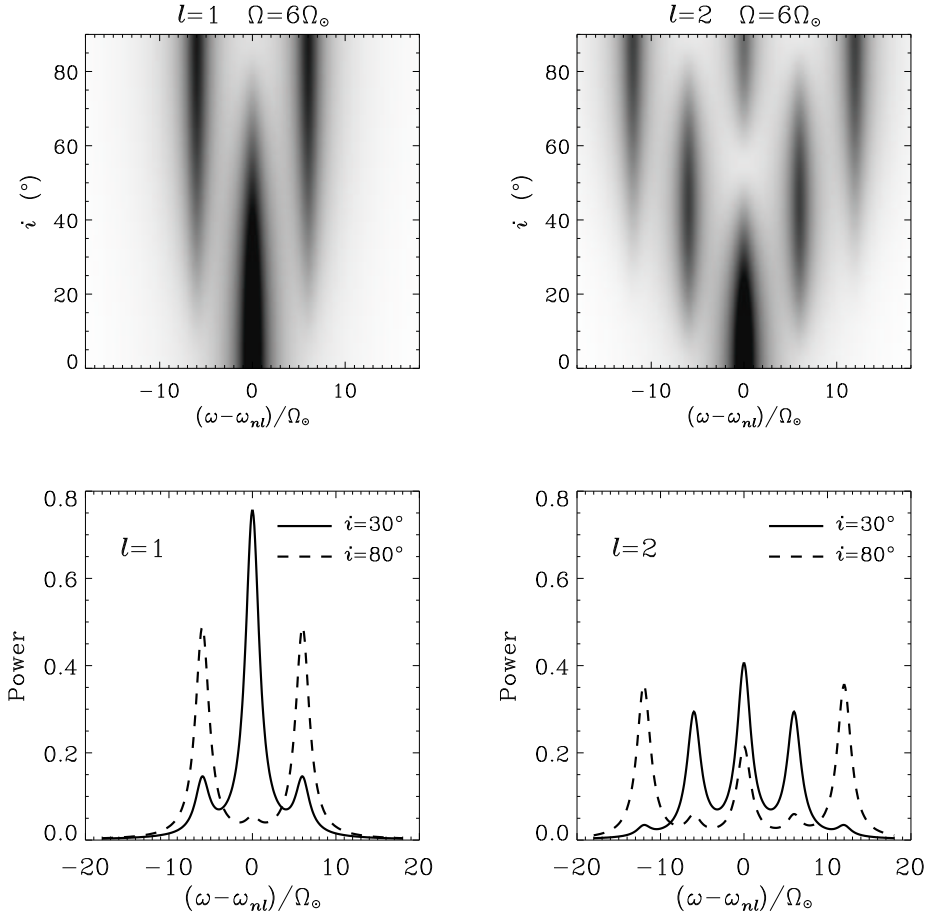


Figure 4.2: Expectation value of the power spectrum, $\mathcal{P}(\omega)$, for dipole and quadrupole multiplets as a function of the inclination angle i . The left panels are for dipole multiplets, $l = 1$, and the right panels are for quadrupole multiplets, $l = 2$. The parameters are $\Gamma = \Gamma_{\odot}$ and $\Omega = 6\Omega_{\odot}$, where $\Gamma_{\odot}/2\pi = 1 \mu\text{Hz}$ and $\Omega_{\odot}/2\pi = 0.5 \mu\text{Hz}$ are characteristic solar values for the line width and the angular velocity. The bottom panels show the power for the specific values $i = 30^{\circ}$ (solid lines) and $i = 80^{\circ}$ (dashed lines). There is no background noise in these plots.

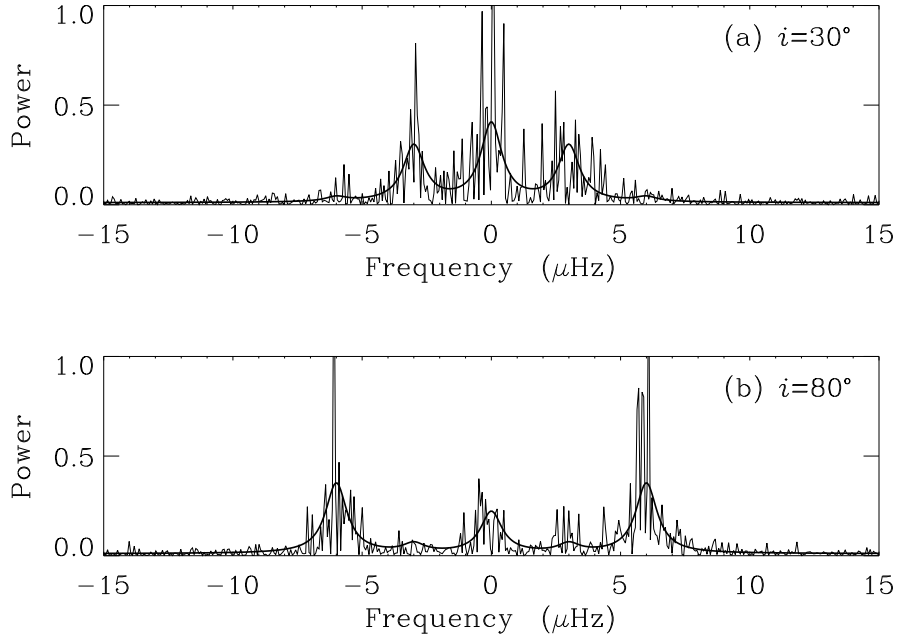


Figure 4.3: Two realizations of the power spectrum of an $l = 2$ multiplet versus centered frequency $(\omega - \omega_{nl})/2\pi$. The stellar rotation is $\Omega = 6\Omega_{\odot}$ and the mode line width is $\Gamma = \Gamma_{\odot}$. Panel (a) corresponds to an inclination angle $i = 30^{\circ}$ and panel (b) is for $i = 80^{\circ}$. A signal-to-noise ratio $S/N=100$ has been prescribed and the simulation corresponds to 6 months of uninterrupted observations. The expectation value of the power, \mathcal{P} , is overplotted (smooth curves).

are equal to their maximum likelihood estimates:

$$\boldsymbol{\lambda}^* = \underset{\boldsymbol{\lambda}}{\operatorname{argmin}} \{ \mathcal{L}(\boldsymbol{\lambda}) \} . \quad (4.30)$$

We use the conjugate gradient method to find the parameters that minimize the function \mathcal{L} .

The method of maximum likelihood has many good properties (e.g. Kendall & Stuart, 1967; Rao, 1973). The maximum likelihood estimate $\boldsymbol{\lambda}^*$ is not biased as the sample size tends to infinity. Moreover, for large sample size, $\boldsymbol{\lambda}^*$ will have an approximate multi-normal distribution centered on the true parameter value $\boldsymbol{\lambda}$. Maximum likelihood estimators are also minimum variance estimators. Furthermore when the model is misspecified, $\boldsymbol{\lambda}^*$ will still have a well-defined probability distribution and will be approximately normally distributed. In our case we have a finite sample size, since T is limited to a few months. There is no guarantee that the maximum likelihood estimator will be normally distributed or even unbiased. Note also that the distribution of i^* has to be periodic since \mathcal{L} only depends on $|i| \bmod \pi$.

In order to derive the correct probability distributions of the likelihood estimates, we run Monte-Carlo simulations (e.g. Toutain & Appourchaux, 1994). The method consists of simulating a large number of realizations of a power spectrum and then fitting each realization to construct the distribution of the measured λ_k^* . Monte-Carlo simulations enable us to determine the bias and the precision associated with the measurement of each parameter λ_k . Ideally we would want to run simulations for each relevant point in $\boldsymbol{\lambda}$ -space and for varying observation times T . Because Monte-Carlo simulations are time consuming, we decide to keep Γ and S/N fixed to their solar values, varying only Ω and i . For all simulations, the observation time is $T = 6$ months.

4.1.4 Results

In Figure 4.4 we show the results for one set of Monte-Carlo simulations. Plotted are in Figures 4.4a and 4.4c the inclination angle i^* , and in Figures 4.4b and 4.4d the angular velocity in solar units, Ω^*/Ω_\odot , returned by the fit versus the inclination angle, i , that entered the computation of each realization. For this set we simulate

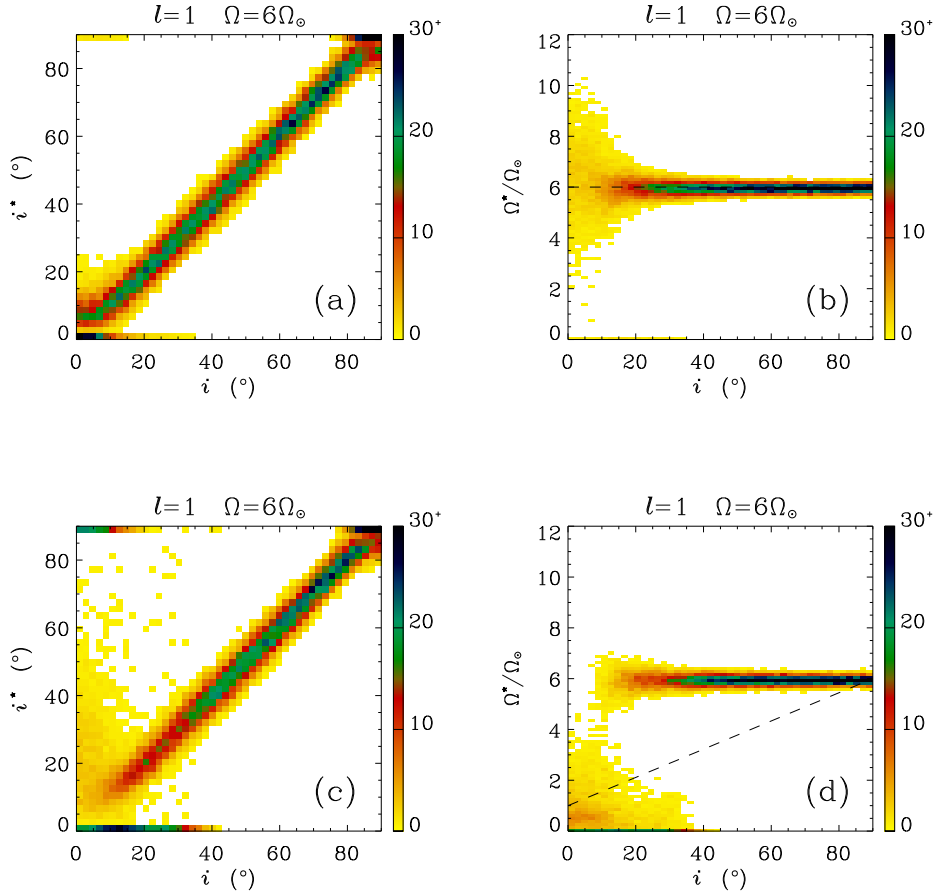


Figure 4.4: Maximum likelihood estimates i^* and Ω^* deduced from an $l = 1$ triplet versus the true i . The true rotation frequency is $\Omega = 6\Omega_\odot$. Plotted are the results of 2000 realizations. Panels (a) and (b) differ from (c) and (d) in the initial guess for the rotation rate (indicated by the dashed lines). The scale indicates the percentage of the points falling into a bin. For (a) and (c) a bin is 2 deg. For (b) and (d) a bin is $0.12\Omega_\odot$.

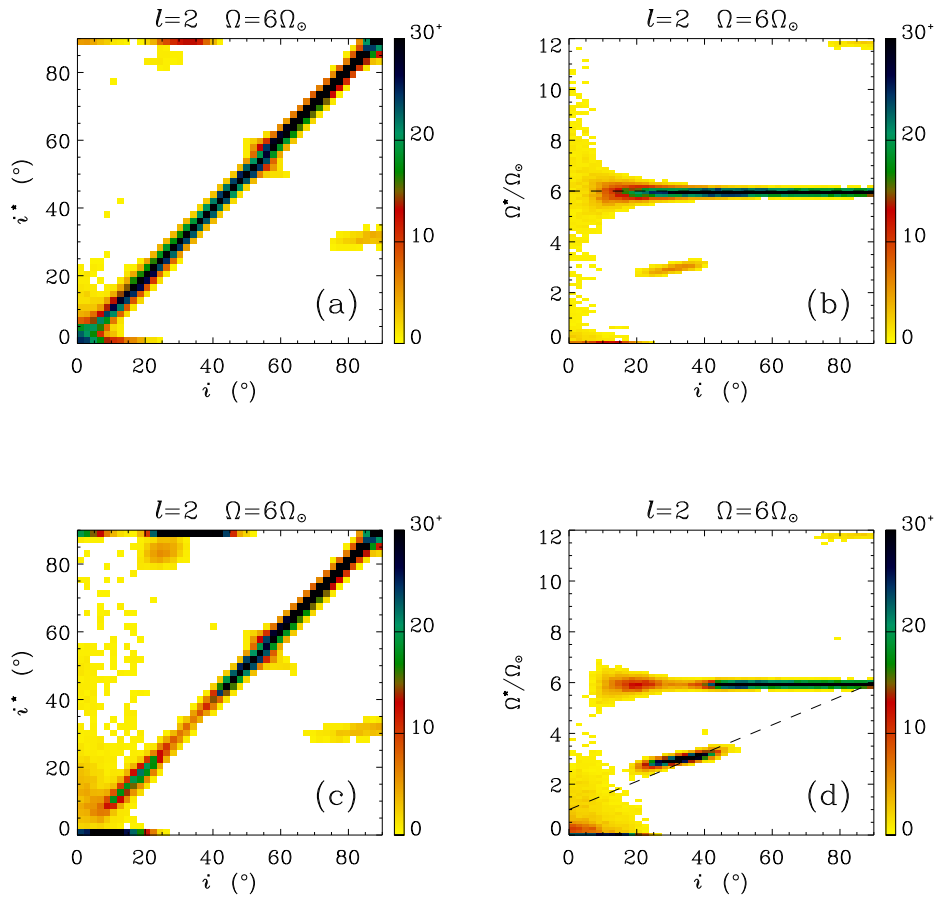


Figure 4.5: The same as Figure 4.4, but for an $l = 2$ multiplet.

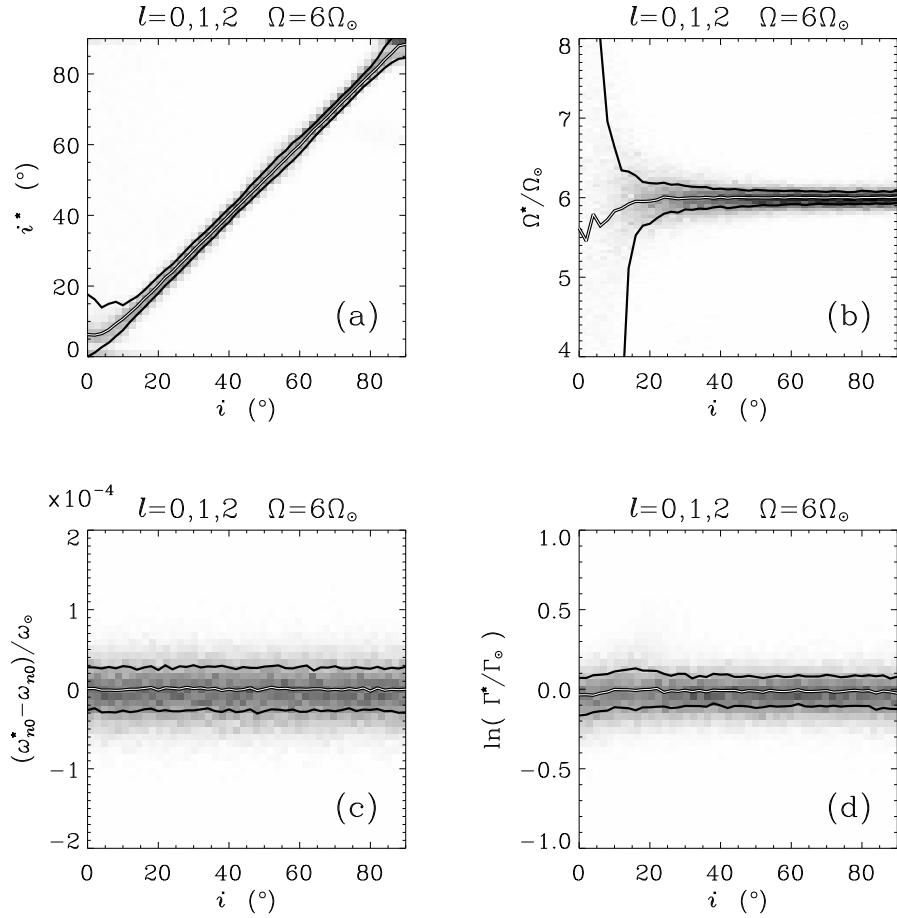


Figure 4.6: Maximum likelihood estimates obtained by fitting three multiplets $l = 0, 1, 2$ simultaneously, for $\Omega = 6\Omega_{\odot}$. The gray scale shows the distributions of i^* , Ω^* , the full width at half maximum, Γ^* , and the frequency of the $l = 0$ mode, ω_{n0}^* , versus i . Plotted are the results of 750 realizations. The thin double lines mark the median of the estimated parameters for each i , and 2/3 of the points fall in between the two thick lines.

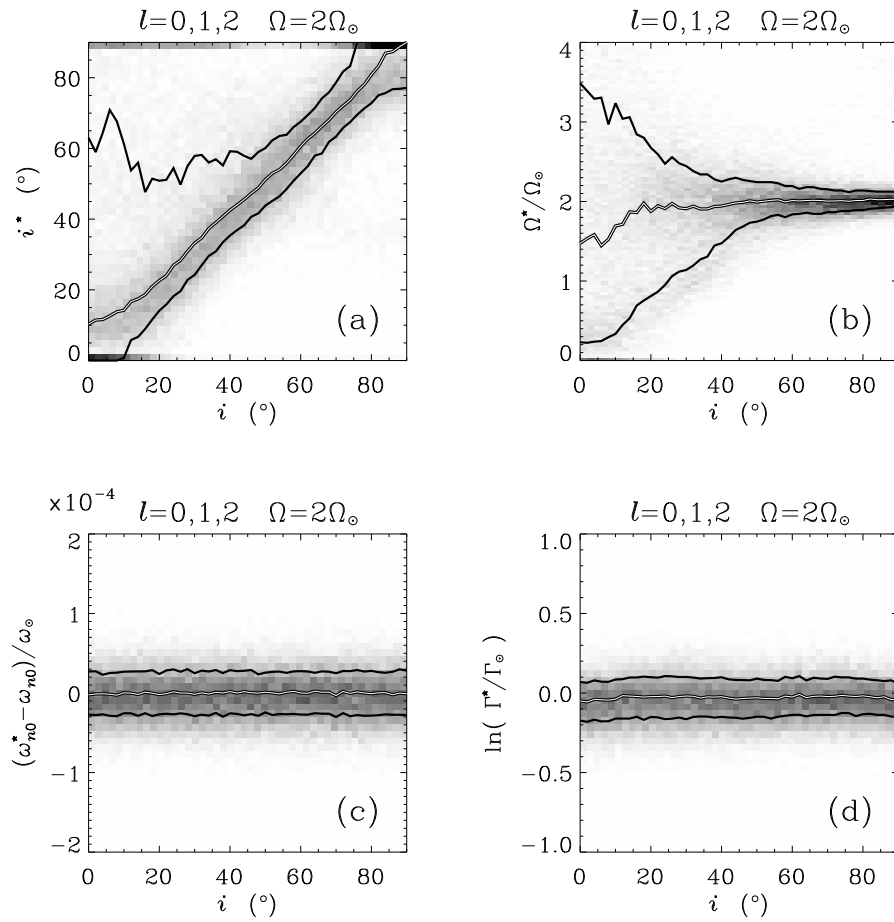


Figure 4.7: Same as Figure 4.6 but for $\Omega = 2\Omega_{\odot}$

a single $l = 1$ triplet and the rotation frequency is $\Omega = 6\Omega_{\odot}$. For each value of the inclination angle i ranging from 0 to 90° , we computed 2000 realizations of the power spectrum. The initial guesses in ω_{nl}^* , Γ^* , S^* , and N^* for the fits to the simulated spectra are randomly distributed in some interval around the true parameter values. The random initial guess in i^* is uniformly distributed between 0 and 90° , whatever the true inclination angle. For Ω^* , we started with two different initial guesses. The guesses are indicated by the dashed lines in Figure 4.4b (for the results shown in Figures 4.4a and 4.4b) and 4.4d (for Figures 4.4c and 4.4d). The guess for Ω shown in Figure 4.4d is not too dissimilar from an initial guess based on $v \sin i$ measurements.

We note that most i^* values returned by the fits lie within $\pm 5^{\circ}$ of the true i . However, the distribution of i^* is highly non-Gaussian as i tends to either 0 or 90° . The accuracy is lower for small i values in particular if a wrong initial guess of Ω^* is made (Figure 4.4c). In this case the fits tend to either $i^* = 0$ or $i^* = 90^{\circ}$ for $i \lesssim 10^{\circ}$. The inaccuracies in Ω^* are also largest for small i , and systematically too low values are returned if the initial guess is too low (Figure 4.4d).

The reason for this behavior lies in the fact that only the $m = 0$ component is visible at $i \approx 0$ (Figure 2). Hence the oscillation spectrum does not provide any means of distinguishing between a (rapidly) rotating star observed almost pole on and a non-rotating (or very slowly rotating) star with arbitrary i value. In this case the maximum likelihood fit returns the solution closer to the initial guess (compare Figures 4.4b and 4.4d).

In Figure 4.5 we plot the same as Figure 4.4, but for an $l = 2$ mode. On the whole, the results look similar. At most inclination angles the accuracy in the measurements of i^* and Ω^* is higher than for $l = 1$. The major exception is i in the range 20 - 40° . The fitting procedure cannot decide between $i^* \approx i$, $\Omega^* \approx \Omega$ and $i^* \approx 90^{\circ}$, $\Omega^* \approx \Omega/2$. Figure 2 again reveals the cause of this uncertainty. For $i \approx 20$ - 40° only the $m = 0$ and $m = \pm 1$ components have significant power. The solution with $\Omega^* \approx \Omega/2$ is achieved if the $m = \pm 1$ components are misidentified as $\Delta m = \pm 2$. This is only possible if simultaneously $i^* \approx 90^{\circ}$ is assumed (see Figure 2). Unsurprisingly, this wrong solution is more commonly obtained when the initial guess of Ω^* is closer to $\Omega/2$ than to Ω (Figure 4.5d). For $i \gtrsim 80^{\circ}$ again two

solutions are obtained, the correct one and $\Omega^* \approx 2\Omega$ combined with $i^* \approx 30^\circ$. In this case the fitting procedure misidentifies the $m = \pm 2$ peaks as $m = \pm 1$ peaks.

The most reliable result is obtained by fitting dipole and quadrupole modes simultaneously. Figure 4.6 shows likelihood estimates for three multiplets $l = 0, 1, 2$ combined. The ambiguities at $i \approx 20\text{-}40^\circ$ and $i \gtrsim 80^\circ$ present in the fits to $l = 2$ alone are removed, while the scatter in i^* and Ω^* is considerably smaller than for fits to $l = 1$ peaks alone. Only the ambiguity at $i \lesssim 10^\circ$ remains. “Medians” and “error bars” are plotted in Figure 4.6. By construction 2/3 of the points lie between error bars. Because the distributions of i^* and Ω^* are definitely not Gaussian these values are only indicative; they are not sufficient to assess the measurement precision. Also plotted in Figures 4.6c and 4.6d are the fitted frequency of the $l = 0$ mode, ω_{n0}^* , and the line width, Γ^* , common to all the modes. The measurement accuracy of these parameters appears to be independent of the inclination angle i . Indeed rotation has no effect on the singlet $l = 0$. Including an $l = 0$ mode in the minimization procedure helps in turn to measure Ω^* and i^* from the dipole and quadrupole modes by reducing the uncertainty on Γ^* .

So far we have only considered rapidly rotating stars with rotational splitting considerably larger than the line width. We now turn to the case $\Omega = 2\Omega_\odot$ and repeat the analysis described above for $\Omega = 6\Omega_\odot$. The distribution of i^* and Ω^* obtained by fitting 750 realizations to $l = 0, 1, 2$ combined is shown in Figure 4.7. As expected, the accuracy of the deduced i^* and Ω^* values is considerably lower now than for the more rapidly rotating stars. The individual azimuthal components in a multiplet are not resolved since $\Omega = 2\Gamma$. For $i \gtrsim 45^\circ$ the errors are found to be around $\pm 10^\circ$ for i^* and 5-15% for Ω^*/Ω . At smaller i values the fits tend to overestimate i and the uncertainty for both i^* and Ω^* becomes excessively large for decreasing i , but remains unchanged for ω_{n0}^* and Γ^* . A comparison with Figure 4.7 reveals that the accuracy of these last two quantities is mostly independent of the rotation rate when $l = 0, 1, 2$ are fit together.

Although extremely useful, Monte-Carlo simulations require long computations. A less reliable but straightforward method to obtain a formal error, σ_k , on the maximum likelihood estimate λ_k^* is to expand \mathcal{L} about the true parameter value λ_k . As mentioned earlier, in the limit of infinite sample size, $\boldsymbol{\lambda}^*$ tends to a multi-normal

probability distribution which is asymptotically unbiased,

$$\mathbb{E}[\lambda_k^*] = \lambda_k, \quad (4.31)$$

and has minimum variance. An estimate of σ_k is

$$\sigma_k^2 = 1/C_{kk}, \quad (4.32)$$

where C_{kk} is the k -th element on the diagonal of the inverse, $\mathbf{C} = \mathbf{H}^{-1}$, of the Hessian matrix given by

$$H_{kk'} = \mathbb{E} \left[\frac{\partial^2 \mathcal{L}}{\partial \lambda_k \partial \lambda_{k'}}(\boldsymbol{\lambda}) \right]. \quad (4.33)$$

The formal error σ_k , called the Cramer-Rao lower bound, is a lower limit on the error bar associated with the measurement of λ_k (e.g. Kendall & Stuart, 1967). Toutain & Appourchaux (1994) showed that these error bars are useful estimates in helioseismology.

Figure 4.8 shows the errors $\sigma_{\sin i}$ and σ_Ω derived from equation (4.32) for a single $l = 1$ mode, plotted as a function of $\sin i$ and Ω/Ω_\odot . This calculation is easier to carry out when $\sin i$ is chosen as an independent parameter instead of i . A comparison with Figures 4.6 and 4.7 reveals that the error bars obtained by inverting the Hessian have the correct magnitude. By construction they are symmetric about the true parameter values and they cannot describe the asymmetric distribution of i^* displayed by the Monte Carlo simulations (Figure 4.7). Of particular interest is the dependence of the error bars on Ω . Figure 4.8 suggests that it is extremely difficult to determine either i or Ω for a star with the solar rotation rate when a single mode $l = 1$ is taken into consideration.

We have also determined error bars from Monte-Carlo simulations for stellar rotation frequencies in the range $1 < \Omega/\Omega_\odot < 10$, although restricted to only $i = 30^\circ$ and 80° . Medians and error bars are plotted in Figure 4.9 for a simultaneous fit to three multiplets, $l = 0, 1, 2$. This figure shows that it is realistic to apply asteroseismic techniques for $\Omega \gtrsim 2\Omega_\odot$, with the results being more reliable for $i = 80^\circ$ than $i = 30^\circ$. When azimuthal modes are fully resolved (say $\Omega > 3\Omega_\odot$), error bars are fairly independent of the rotation rate. Note that for $i = 30^\circ$ and

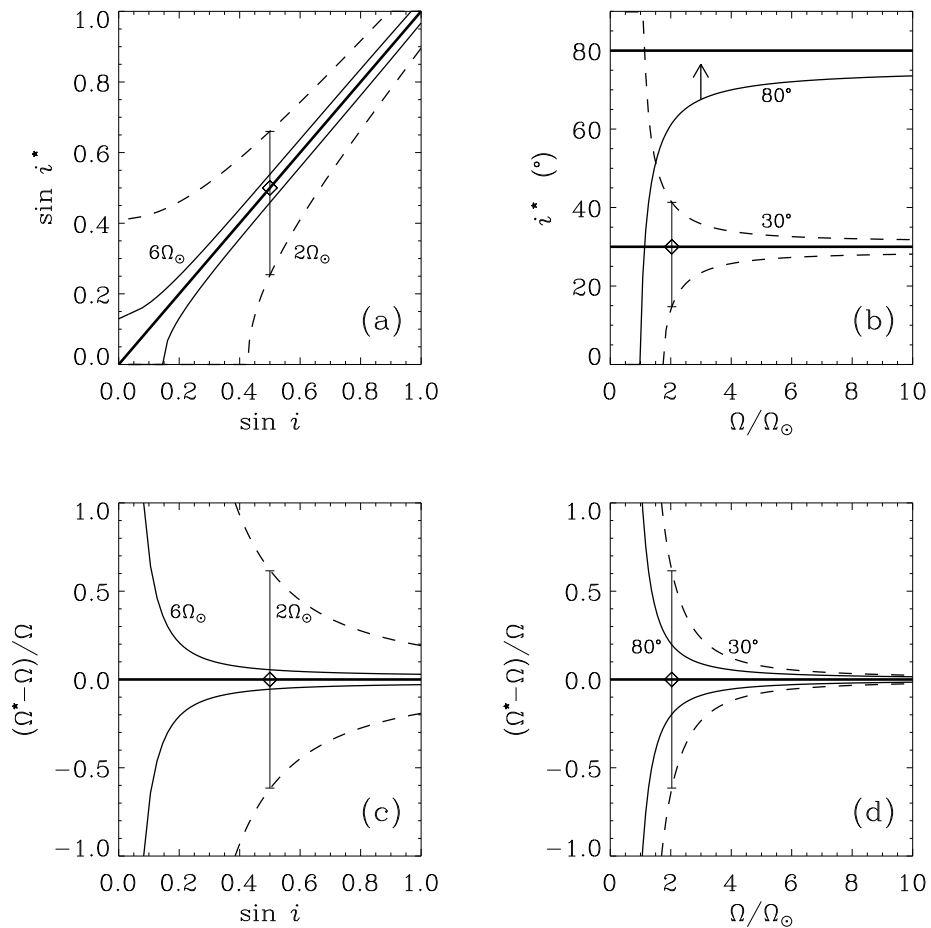


Figure 4.8: Formal error bars obtained by inverting the Hessian for an $l = 1$ multiplet. In panels (a) and (c) the error bars on i^* and Ω^* versus $\sin i$ are given for two rotation rates, $\Omega = 2\Omega_\odot$ (dashed curves) and $\Omega = 6\Omega_\odot$ (solid). In panels (b) and (d) error bars for $i = 30^\circ$ (dashed) and $i = 80^\circ$ (solid) are plotted versus Ω/Ω_\odot . A sample error bar for $\Omega = 2\Omega_\odot$ and $i = 30^\circ$ is explicitly plotted. Other parameters are $\Gamma = \Gamma_\odot$, $S/N = 100$, and $T = 6$ months.

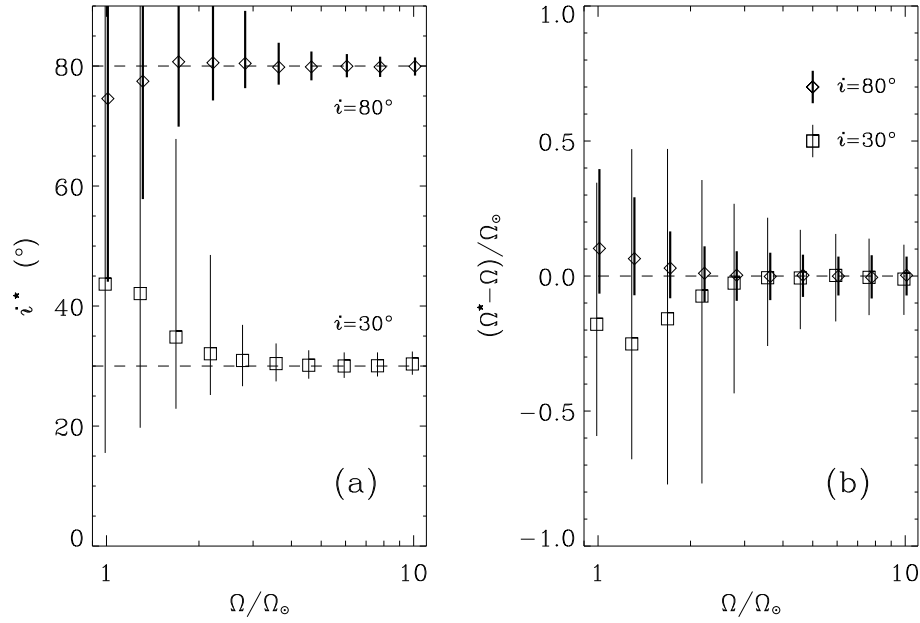


Figure 4.9: Median and error bars for maximum likelihood estimates i^* and $(\Omega^* - \Omega)/\Omega_\odot$ deduced from Monte Carlo simulations as a function of rotation rate. Results are shown for two input inclinations, $i = 30^\circ$ (squares and thin error bars) and $i = 80^\circ$ (diamonds and thick error bars). Three multiplets $l = 0, 1, 2$ are fit together. $\Gamma = \Gamma_\odot$, $S/N = 100$, and $T = 6$ months.

$\Omega < 2\Omega_\odot$, the error bars on Ω (Figure 4.9b) appear to be decreasing for decreasing Ω . This is an artifact: we simply do not have enough realizations to describe the broad distribution of Ω^* in this range. Also, likelihood estimates i^* and Ω^* appear to be biased when $\Omega \lesssim 2\Omega_\odot$. This is likely to be due to our definition of the median (we do not take into account the periodic nature of the distributions).

4.2 Stellar Asphericity

4.2.1 Introduction

Magnetic activity affects the structure of the Sun. These changes are reflected in the observed shifts of the eigenfrequencies of the global modes of solar oscillations (Woodard & Noyes, 1985). Mode frequencies increase with magnetic activity: over the period of the 11-year solar cycle, low-degree modes show fractional frequency shifts of the order of 10^{-4} . Acoustic wave propagation may be affected directly by the magnetic field and/or indirectly through thermal and density changes. The study of high-degree modes has revealed that frequency shifts are caused by structural perturbations confined to the near solar surface and localized in latitude (Libbrecht & Woodard, 1990). The latitudinal dependence can be inferred from the observation that modes with different azimuthal orders, m , are shifted by different amounts. Sound-speed asphericity inversions of high-precision helioseismic data show latitudinal variations that match the butterfly diagram (Antia et al., 2001).

Thanks to Doppler imaging (e.g. Rice, 2002) the spatial distribution of starspots on a rapidly rotating star can be recovered from a series of high-resolution spectral line profiles. Many stars are found to exhibit large polar cap features. Theoretical work by Schüssler & Solanki (1992) indicates that magnetic flux should emerge at high latitudes for fast rotators. However, axisymmetric features such as polar spots do not introduce wavelength variability in the line profiles. For this reason, doubts have been raised about their reality.

Can we learn about the surface distribution of magnetic activity on a star other than the Sun by studying the frequencies of its global modes of oscillation? For distant stars, only modes with spherical harmonic degrees $l \leq 3$ can be observed. As a result wave-speed asphericity inversions will have poor resolution in latitude. In this section we ask whether it might be possible to discriminate between two simple activity configurations: an equatorial band and a polar cap. Asteroseismology will heavily rely on the long and continuous observations provided by the future European space missions COROT and Eddington.

4.2.2 Asphericities

We consider a rotating Sun-like star subject to near-surface structural perturbations introduced by magnetic activity. For perturbations that are steady in an inertial frame, the frequencies of oscillations may be written as

$$\omega_{nlm} = \omega_{nl} + \delta\omega_{nlm}^{(\text{rot})} + \delta\omega_{nlm}^{(\text{AR})} . \quad (4.34)$$

Here the central frequency ω_{nl} includes all spherically symmetric distortions. The rotation-induced frequency splitting is denoted by $\delta\omega_{nlm}^{(\text{rot})}$, and the frequency perturbation due to near-surface magnetic activity is $\delta\omega_{nlm}^{(\text{AR})}$. The activity perturbations have to be azimuthally symmetric with respect to the rotation axis.

In the case of a rigidly rotating star with angular velocity Ω , and up to a second order of approximation, the m -dependent rotational frequency perturbation is approximated by (Dziembowski & Goode, 1992; Kjeldsen et al., 1998):

$$\delta\omega_{nlm}^{(\text{rot})} = m(1 - C_{nl})\Omega + \frac{\Omega^2 R^3}{\mathfrak{G}M} \omega_{nl} Q_{lm} , \quad (4.35)$$

where R is the stellar radius, M is the stellar mass, \mathfrak{G} is the universal constant of gravity, and C_{nl} is the Ledoux constant whose value depends on the oscillation eigenfunctions of the non-rotating star. The second term in Eq. (4.35) describes the P_2 -distortion of the stellar surface due to centrifugal forces, with Q_{lm} given by (Kjeldsen et al., 1998):

$$Q_{lm} \simeq \frac{2/3 \int_{-1}^1 P_2(x) [P_l^m(x)]^2 dx}{\int_{-1}^1 [P_l^m(x)]^2 dx} . \quad (4.36)$$

The P_l^m are associated Legendre functions and P_2 is a second-order Legendre polynomial.

There is no definitive theory for estimating the frequency shifts introduced by near-surface magnetic activity. Here, we separate the physics from the geometry, and parameterize the frequency perturbation in the form

$$\delta\omega_{nlm}^{(\text{AR})} \simeq \omega_{nl} \epsilon_{nl} G_{lm} . \quad (4.37)$$

In this expression, ϵ_{nl} gives the overall (unspecified) amplitude of the fractional frequency shifts. In the Sun, $\epsilon \simeq 10^{-4}$. The m -dependent coefficient G_{lm} is a geometrical weight factor that depends on the latitudinal distribution of surface activity:

$$G_{lm} = \int_{\text{AR}} |Y_l^m(\theta, \phi)|^2 \sin \theta \, d\theta \, d\phi, \quad (4.38)$$

where AR refers to the axisymmetric area covered by magnetic “active regions”. The Y_l^m are normalized spherical harmonics, and θ and ϕ are spherical-polar coordinates defined in the inertial frame with polar axis pointing in the direction of the rotation axis.

For a given multiplet (l, n) , the mode frequencies ω_{nlm} can be expressed in terms of a unique set of $2l + 1$ so-called a -coefficients:

$$\omega_{nlm} = \sum_{j=1}^{2l+1} a_j(n, l) \mathcal{P}_j^{(l)}(m), \quad (4.39)$$

where the polynomials $\mathcal{P}_j^{(l)}(m)$ form an orthogonal set. The standard polynomials used in this expansion are describe by Schou et al. (1994). For quadrupole multiplets, the expansion up to a_2 is:

$$\omega_{n2m} = \omega_{n2} + m a_1(n, 2) + (m^2 - 2) a_2(n, 2) + \dots \quad (4.40)$$

The coefficient a_1 relates to the first-order effect of rotation, with $a_1 \simeq \Omega$ in the case of rigid-body rotation. The coefficient a_2 is a measure of asphericity and includes magnetic and second-order rotational effects. Rotational oblateness implies $a_2 < 0$. Because wave-speed is increased in active regions, an equatorial band of activity would tend to reduce the effective oblateness, i.e. to increase a_2 . Polar activity, on the other hand, decreases the value of a_2 . In the Sun, activity migrates equatorward as the cycle develops and the coefficient a_2 is about 35 nHz higher at solar maximum than at minimum (Appourchaux, 2002).

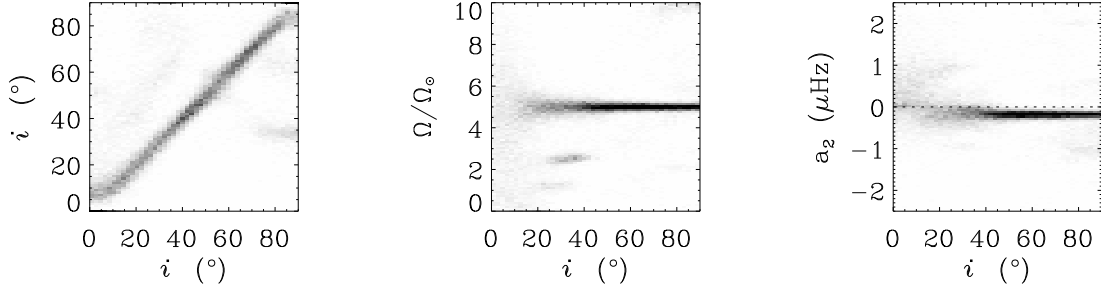


Figure 4.10: Maximum likelihood estimates of i , Ω and a_2 deduced from an $l = 2$ multiplet versus the true inclination angle. The star is solar-like with angular velocity $\Omega = 5\Omega_\odot$. The negative value of a_2 is entirely due to rotational oblateness (no magnetic perturbation was introduced). Observation time $T = 6$ months.

4.2.3 Equatorial Band vs. Polar Cap

The precision of the measurement of the asphericity parameter a_2 depends on the input stellar parameters and is limited by realization noise (stellar pulsations are forced by turbulence). Like before we simulate a large number of realizations of an oscillation power spectrum for a given stellar configuration, then extract oscillation parameters using a maximum likelihood technique, and derive the distribution of the measured values of a_2 .

For this preliminary study we consider a solar-like star with solar mass and radius and uniform angular velocity $\Omega = 5\Omega_\odot$, where $\Omega_\odot = 0.5 \mu\text{Hz}$. Mode visibility is a function of the inclination angle, i , between the line of sight and the stellar rotation axis. Ignoring activity-related changes in the mode eigenfunctions, the observed power in individual m -components is given by:

$$\mathcal{E}_{lm}(i) = \frac{(l - |m|)!}{(l + |m|)!} [P_l^m(\cos i)]^2 . \quad (4.41)$$

Each mode is assumed to have a Lorentz profile with full width at half maximum $\Gamma = 1 \mu\text{Hz}$, and the signal-to-noise ratio in the power spectrum is $S/N = 20$, i.e. one fifth of the solar value. The observation time interval is $T = 6$ months. As mentioned earlier we restrict our attention to two basic configurations: a polar cap $45^\circ < \lambda < 90^\circ$ and an equatorial band $-8.4^\circ < \lambda < 8.4^\circ$, where $\lambda = \pi/2 - \theta$ is the latitude. Activity covers the same area in both cases. The amplitude of the magnetic perturbation, ϵ , remains a variable parameter with values up to 10^{-3} . For

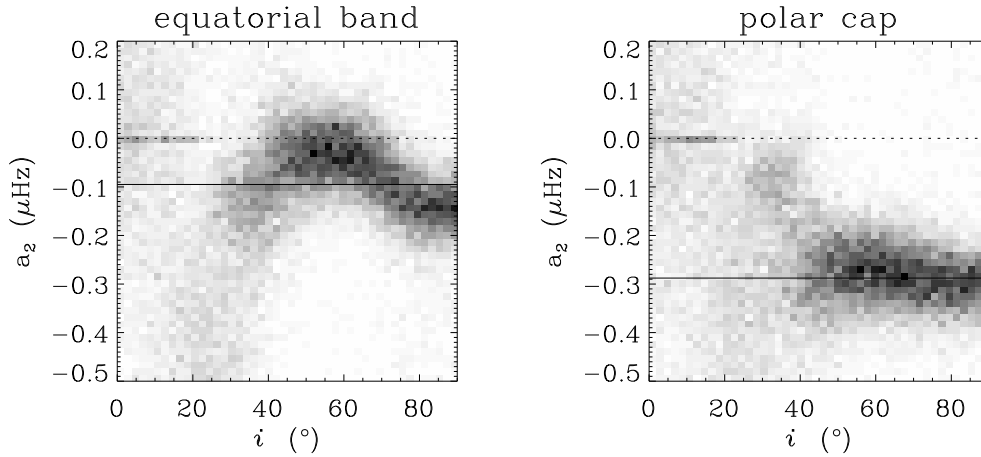


Figure 4.11: Maximum likelihood estimates of the asphericity parameter a_2 versus inclination angle for an $l = 2$ multiplet. In the left panel, activity is restricted to an equatorial band, and in the right panel to a polar cap. The activity-related fractional frequency shift is $\epsilon = 5 \times 10^{-4}$. Solid lines refer to the true a_2 .

each inclination angle, we simulate 1000 realizations of the power spectrum for a single $l = 2$ multiplet.

Using a maximum likelihood technique (e.g. Toutain & Appourchaux (1994)), we fit a parametric model to each simulated power spectrum, which depends on ω_{n2} , Ω , a_2 , Γ , i and the overall signal and noise levels. Figure 4.10 shows, for $\epsilon = 0$, the distributions of the estimates of i , Ω , and a_2 returned by the fit, as a function of the true inclination angle i . The fit works reasonably well for $i > 40^\circ$. For $i < 20^\circ$ rotation cannot be inferred with sufficient precision. In the range $20^\circ < i < 40^\circ$, the $m = \pm 1$ modes are sometimes misidentified as $m = \pm 2$ modes. Rotational oblateness can be retrieved for $i > 40^\circ$.

Figure 4.11 shows the values of a_2 returned by the fit when the activity perturbation is switched on. For $\epsilon = 5 \times 10^{-4}$ and $i > 40^\circ$, it is possible to distinguish a polar cap of activity from an equatorial band of activity. Note that the estimate of a_2 may be significantly biased. There are two reasons for this bias: (1) all 5 modes are not visible simultaneously and (2) the model of the power spectrum is misspecified (we do not fit for a_4). Figure 4.12 shows that for $i = 60^\circ$ the parameter a_2 can be measured from a single $l = 2$ multiplet with a precision of ± 50 nHz. The distinction between the two configurations can only be made if $\epsilon > 5 \times 10^{-4}$.

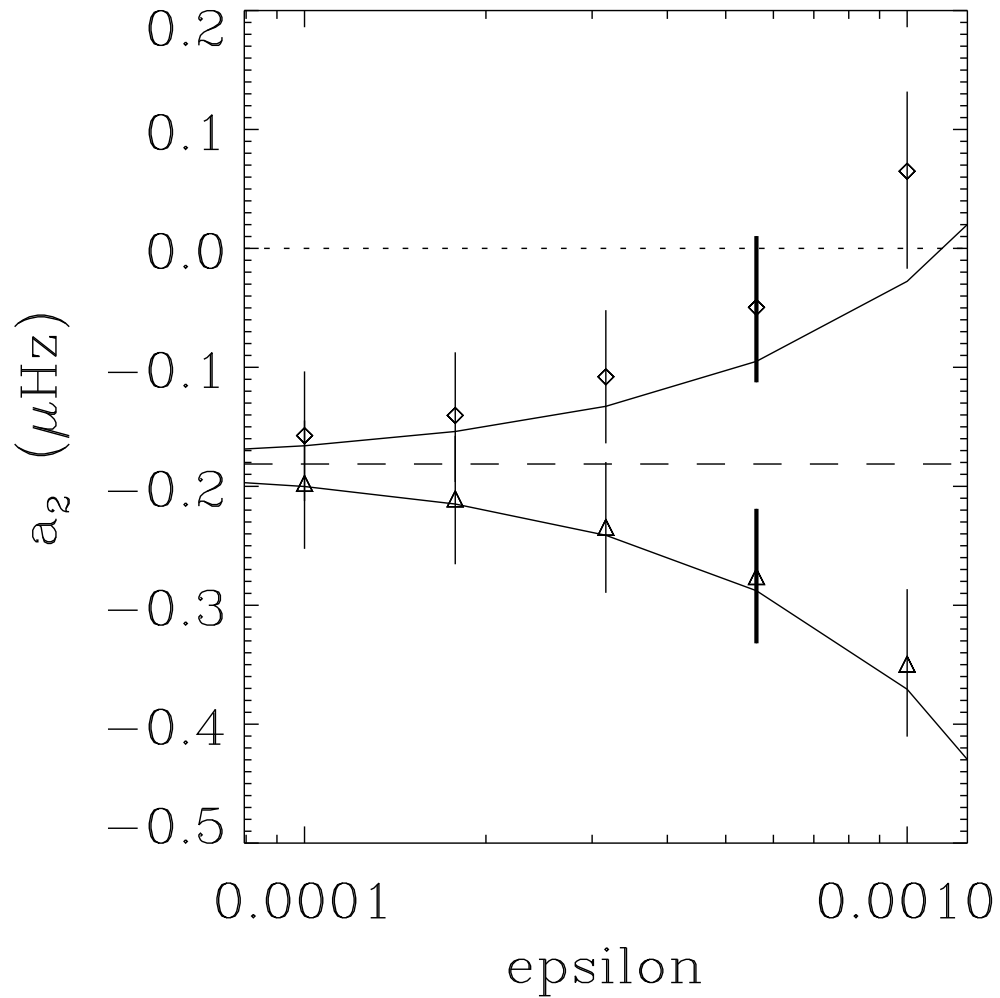


Figure 4.12: Mean and standard deviation of measured a_2 versus ϵ at inclination angle $i = 60^\circ$ and for $l = 2$. Equatorial band of activity (diamonds) and polar cap (triangles). Solid lines refer to the true a_2 . The dashed line is the rotational oblateness value ($\epsilon = 0$).

We have seen that stellar oscillations may contain measurable information about the latitudinal distribution of stellar activity. Stellar rotation must be large enough (individual m -components must be resolved), stellar activity must be strong enough (say $\epsilon > 5\epsilon_{\odot}$), and the inclination angle of the star must be large enough (say $i > 40^{\circ}$).

Both rotational oblateness and aspherical magnetic perturbations contribute to the value of the parameter a_2 . In order to detect the asphericity due to activity alone, it is necessary to remove the oblateness due to rotation. To do so, one must estimate $\Omega^2 R^3 / \mathcal{G}M$. Hopefully, Ω can be measured from the frequency splittings and the mean stellar density M/R^3 can be deduced from the large frequency separation $\omega_{nl} - \omega_{n-1,l} \propto \sqrt{R^3/M}$ (Brown & Gilliland, 1994).

The present study is however not appropriate for a long-lived patch of activity that would be localized in longitude, because such a perturbation is unsteady in the inertial frame of the observer. The signature of an unsteady magnetic perturbation in oscillation power spectra is rather complicated. An example for the Sun is provided by Gizon (1998) who studied the perturbation arising from the presence of a large rotating “sunspot”. In this case the power spectrum of a given multiplet (l, n) displays $(l+1)(2l+1)$ peaks, most of which cannot be resolved.